M. Toya[1]
Professor
Department of Mechanical Engineering,
Graduate School of Science and Engineering,
Kagoshima University,
1-21-40, Korimoto,
Kagoshima 890-0065, Japan
e-mail: toyamasa@mech.kagoshima-u.ac.jp

K. Fukagawa
Lecturer
Department of Technology Education,
Faculty of Education,
Kagoshima University,
1-20-6, Korimoto,
Kagoshima 890-0065, Japan

M. Aritomi
Associate Professor

M. Oda
Assistant Professor

T. Miyauchi

Department of Mechanical Engineering,
Graduate School of Science and Engineering,
Kagoshima University,
1-21-40, Korimoto,
Kagoshima 890-0065, Japan

Local Delamination Buckling of a Laminated Beam due to Three-Point Bending

Asymmetric three-point bending of a layered beam containing an interior interface crack is analyzed on the basis of the classical beam theory. Axial compressive and tensile forces are induced by bending in the parts of the beam above and below the delamination, and they are determined by modeling the cracked part as two lapped beams jointed together at the corners of both beams. When the magnitude of the applied load is small, the beam deflects, retaining the mutual contact of whole crack faces, but as the applied load reaches a critical value, local delamination buckling of the compressed part occurs. The relation between the magnitude of the applied load and the deflection at the point of load application is found to be nearly bilinear. The validity of this prediction is confirmed by experiments. It is also shown that once the delamination buckling occurs, the energy release rate generally becomes larger as compared with the case of a perfect contact of delaminated surfaces. [DOI: 10.1115/1.4001444]

Keywords: laminated beams, delamination, buckling, three-point bending, energy release rates

1 Introduction

Fiber-reinforced materials are usually utilized as laminates, but such laminated beams or plates often contain interior delaminations, or interface cracks, which are introduced easily by low-velocity impact normal to the surface of laminates or from manufacturing errors in the bonding process. To make clear the conditions for the growth of initial interior delaminations is important for practical applications of laminates. Consequently, many literatures have been presented on the delamination of laminated materials.

Maikuma et al. [1] studied the problem where an interface crack at the center of a laminated beam made by bonding two isotropic beams of equal material properties extends by a symmetrical three-point bending. Suemasu and Majima [2,3] solved the parallel problems where multiple penny-shaped interlaminar delaminations grow under a transverse concentrated force applied at the center of a circular plate. Hutchinson and Lu [4] derived the energy release rate of an internal delamination embedded in an orthotropic beam when it is subjected to temperature gradient. Toya et al. [5] analyzed an edge delamination of a laminated beam subjected to temperature gradient. The present authors [6] also analyzed the asymmetrical three-point bending of a laminated beam consisting of two beams with different elastic properties and containing a delamination along the bond-line. Based on a simple beam theory, closed-form solutions for the deflection of the point of load application were obtained as a function of the applied force and the delamination length. The energy release rate and its mode I and II components at both tips of the delamination were then derived. These analytical results were also confirmed by the numerical analyses based on finite-element analyses.

In our previous model [6] the contact of crack faces was assumed. In a course of experiments to test our theory, however, we found that when the thickness of one constituent beam is thin enough, local delaminaiton buckling occurred when the magnitude of the applied load reaches some critical value. Therefore, our previous analyses based on the assumption of the mutual contact of whole crack faces are valid only up to a certain critical value of applied loads, and the analyses have to be newly conducted for the study of post-buckling behavior of laminated beams.

Many papers treating the local buckling of one-dimensional or circular delaminations in beams or plates caused by uniaxial or axisymmetric in-plane compressive loadings [7–12] have been presented. To the best of the present authors' knowledge, however, the local buckling of delaminations caused by transverse loading has not been presented yet.

In this paper, on the basis of a simple beam theory we study the problem where delaminations in laminated beams cause local buckling by three-point bending (cf. Fig. 1). A nonlinear equation determining the axial forces induced by bending in the parts of the beam above and below the delaminations is derived (Sec. 2). This equation possesses only one solution for small loads, whereas it yields more than two solutions as the applied load becomes large. By examining the deflection curves of the beam corresponding to each solution, it is found that the occurrence of buckling corresponds to the advent of the second solution. Therefore, critical buckling loads may be defined as the load at which the second solution comes to appear first. On the other hand, for loads

[1]Corresponding author.

Contributed by the Materials Division of ASME for publication in the JOURNAL OF ENGINEERING MATERIALS AND TECHNOLOGY. Manuscript received November 30, 2009; final manuscript received March 12, 2010; published online June 16, 2010. Assoc. Editor: Hussein Zbib.

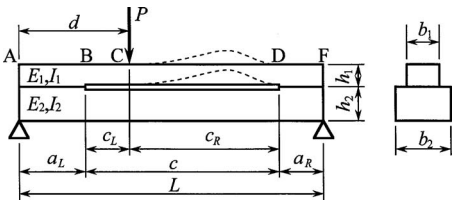

Fig. 1 Three-point bending of a laminated beam containing an interface crack

smaller than the critical load, our previous theory [6] assuming the contact of whole crack faces is effective. Nearly bilinear relations between the applied load and deflection at the point of load application are obtained for some model laminates, which are shown to agree well with the experiments (Sec. 4). The effect of delamination buckling on the energy release rate is also discussed in Sec. 3. It is concluded that the energy release rate generally becomes larger as compared with the case of perfect contact of crack faces due to buckling. Our theory may be extended to orthotropic layered beams if each beam is orthotropic with respect to the beam axis.

2 Analyses of Local Delamination Buckling

2.1 Case Where the Point of Load Application Lies on the Delaminated Region. Analytical model is shown in Fig. 1. The length of the beam (the distance between the two supports) is denoted by L. The height and width of the beam, Young's modulus, and the moment of inertia are denoted by h_i, b_i, E_i, and I_i ($i=1,2$), where suffixes 1 and 2 correspond to the upper and lower beams, respectively. It is assumed that an initial internal delamination (interface crack) with length c is embedded, with the distance of the left-hand and right-hand tips from the left and right-hand supports being a_L and a_R, respectively. Further, a concentrated normal force P is applied at the point distant d apart from the left support (or $d'=L-d$ from the right support). The case where the point of load application lies on the cracked part ($a_L<d<L-a_R$) is considered first. As shown in Fig. 1, the position of load application is distant c_L from the left-side edge of the crack and c_R from the right-side edge ($c=c_L+c_R$).

We cut the beam at points B and D to isolate three elements AB, BD, and DF, and consider the free-body diagrams of each part. The delaminated part BD may be regarded as two lapped beams jointed together at the corners of both beams [6]. The action of the two joints is to produce a horizontal compressive force $-Z$ for the upper beam and extensional force Z for the lower beam, the magnitude of which is later determined from the compatibility condition for the longitudinal deformation of both beams. Also, the joints exert upward and downward forces $\pm R_B$ and $\pm R_D$ at both ends of the beam. By replacing the joints with these forces, we have free-body diagrams of the two upper and lower beams to the delamination, as shown in Fig. 2.

We consider the situation where $c_L<c_R$ and the delaminated surfaces are contacting one another in the interval BC, whereas

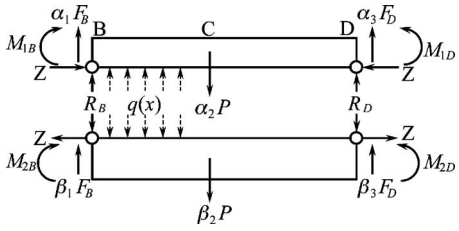

Fig. 2 Analytical model for the delaminated part (free-body diagrams for the interval BD)

the part CD of the upper beam causes local delamination buckling, as depicted by a dashed curve in Fig. 1. Thus mutual beam reactions $\pm q(x)$ act in the interval BC. We assume no frictional forces act on contact surfaces, so that $q(x)$ acts normal to the crack faces. Shearing forces $\alpha_1 F_B$ and $\alpha_3 F_D$, bending moments M_{1B} and M_{1D}, compressive force Z, and upward forces R_B and R_D are applied at the ends of the upper beam in the direction, as shown in Fig. 2. Shearing forces $\beta_1 F_B$ and $\beta_3 F_D$, bending moments M_{2B} and M_{2D}, extensional force Z, and downward forces R_B and R_D likewise act for the lower beam. Here, α_1, α_3, β_1, and β_3 are constants that satisfy the relation $\alpha_1+\beta_1=1$ and $\alpha_3+\beta_3=1$.

To simplify the analyses we a priori assume that the contact region is coincident with the interval BC. But instead, in order to analyze the deflection, we have to assume that a part of the applied load $\alpha_2 P$ acts on the upper beam and $\beta_2 P$ on the lower beam, where $\alpha_2+\beta_2=1$, and the value of α_2 (or β_2) have to be determined in the course of the solution procedure.

The conditions of equilibrium lead to the following equations:

$$F_B = Pd'/L, \quad F_D = Pd/L$$

$$M_{1B} + M_{2B} = F_B a_L, \quad M_{1D} + M_{2D} = F_D a_R \tag{1}$$

In the interval BC, taking the coordinate x with the origin at B, the bending moments M_{x1} and M_{x2} at point x on the neutral axes of the upper and lower beams, are given as follows:

$$M_{x1} = M_1 + \alpha_1' F_B x + Zy(x) + \int_0^x q(x')(x-x')dx' \tag{2}$$

$$M_{x2} = M_2 + \beta_1' F_B x - Zy(x) - \int_0^x q(x')(x-x')dx' \tag{3}$$

where y is the deflection (the positive y is downward), which is assumed to be identical for both beams, and we have put

$$\alpha_1' F_B = \alpha_1 F_B + R_B, \quad \beta_1' F_B = \beta_1 F_B - R_B \tag{4}$$

$$M_1 = M_{1B} - Zh_1/2, \quad M_2 = M_{2B} - Zh_2/2 \tag{5}$$

where $\alpha_1'+\beta_1'=1$. The equations of deflections are

$$D_1 d^2y/dx^2 = -M_{x1}, \quad D_2 d^2y/dx^2 = -M_{x2} \tag{6}$$

with D_i being the flexural rigidity of the upper and lower beams, respectively, i.e., $D_i=E_i I_i$, $I_i=b_i h_i^3/12$ ($i=1,2$). Adding Eq. (6), we have the deflection in the interval BC relative to point B ($x=0$) as follows:

$$y_{BC} = s_1 x^3 + s_2 x^2 + s_3 x \tag{7}$$

where

$$s_1 = -F_B/(6D) \tag{8}$$

$$s_2 = \left(-F_B a_L + \frac{1}{2} hZ\right)/(2D) \tag{9}$$

where $D=D_1+D_2$, $h=h_1+h_2$, and s_3 is an unknown constant. The distribution of the reactive force is obtained as a function of Z

$$q(x) = -Z\frac{d^2 y_{BC}}{dx^2} = \frac{d'PZ}{LD}\left(x + a_L - \frac{LhZ}{2d'P}\right) \tag{10}$$

We also have the end moments M_i ($i=1,2$) given by Eq. (5) as a function of Z

$$M_i = -D_i y''_{BC}|_{x=0} = D_i(F_B a_L - hZ/2)/D \quad (i=1,2) \tag{11}$$

In the interval CD ($d-a_L \le x \le c$), the two beams no longer retain mutual contact due to local buckling, so that $q(x)=0$ and the deflections of the two beams are different from one another. We denote y_1 and y_2 as the deflections of the upper and lower beams,

respectively. Using Eq. (10), we have from Eqs. (2) and (3) the moments at x as follows:

$$M_{x1} = M_1 + \alpha_1' F_B x + f_1 Z - f_2 Z x + Z y_1(x) - \alpha_2 P(x - d + a_L) \tag{12}$$

$$M_{x2} = M_2 + \beta_1' F_B x - f_1 Z + f_2 Z x - Z y_2(x) - \beta_2 P(x - d + a_L) \tag{13}$$

where

$$f_1 = \frac{-F_B(d-a_L)^2}{D}\left[\frac{d-a_L}{3} + \frac{1}{2}\left(a_L - \frac{hZ}{2F_B}\right)\right] \tag{14}$$

$$f_2 = \frac{F_B(d-a_L)}{2D}\left(-d - a_L + \frac{hZ}{F_B}\right) \tag{15}$$

Solving Eq. (6), we obtain

$$y_1 = A_1 \sin(k_1 x) + B_1 \cos(k_1 x) - (M_1 + \alpha_1' F_B x)/Z - f_1 + f_2 x + \alpha_2 P(x - d + a_L)/Z \tag{16}$$

$$y_2 = A_2 \exp(k_2 x) + B_2 \exp(-k_2 x) + (M_2 + \beta_1' F_B x)/Z - f_1 + f_2 x - \beta_2 P(x - d + a_L)/Z \tag{17}$$

where

$$k_1 = \sqrt{Z/D_1}, \quad k_2 = \sqrt{Z/D_2} \tag{18}$$

Taking the coordinate x with the origin at A, the deflections y_{AB} and y_{DF} in the interval AB and DF are given as follows:

$$y_{AB} = -F_B x^3/(6D') + s_4 x \tag{19}$$

$$y_{DF} = \frac{F_D}{6D'}x^3 - \frac{Pd}{2D'}x^2 + s_5 x + s_6 \tag{20}$$

where D' is the flexural rigidity of the composite beam, which may be expressed as [6]

$$D' = D + h^2 D_0/4 \tag{21}$$

with

$$D_0 = 1/[(b_1 E_1 h_1)^{-1} + (b_2 E_2 h_2)^{-1}] \tag{22}$$

Further, from the condition $y_{DF}|_{x=L}=0$, we have

$$s_6 = PdL^2/(3D') - s_5 L \tag{23}$$

The nine unknown constants A_i, B_i $(i=1,2)$, s_3–s_5, α_1', and α_2 are determined as functions of Z from the conditions of continuity of deflections and the angle of inclination at points B, C, and D. They are given in Appendix A.

Finally, we determine the axial force Z. We consider a rectangle in the delaminated part of the beam BD prior to deformation, which consists of the pair of neutral axes of the upper and lower beams to the delamination and the pair of side lines with length $h/2$ connecting both end points of the neutral axes on the cross sections at B and D (cf. Fig. 2). After the jointed beam BD is deformed and local buckling of the delamination occurs, side lines and beam axes still remain perpendicular at all four corner points. On the other hand, the distance BD between the end points of the neutral axis of the upper beam becomes short by the axial compressive force Z and by the effect of curvature induced by bending [7]. Likewise, the distance BD of the neutral axis of the lower beam changes by the axial extensional force Z and by the effect of curvature. The difference between the two distance changes should be equal to $h/2\times$ (sum of the angles of the inclination of the cross sections at points B and D). This condition leads to the following equation for Z:

$$F(Z) = 0 \tag{24}$$

where

$$F(Z) = \frac{Zc}{E_1 h_1 b_1} + \frac{Zc}{E_2 h_2 b_2} + \frac{1}{2}\int_{d-a_L}^{c} (y_1')^2 dx - \frac{1}{2}\int_{d-a_L}^{c} (y_2')^2 dx - \frac{h}{2}(\theta_L + \theta_R) \tag{25}$$

with θ_L and θ_R being the angles of inclination at points B and D

$$\theta_L = \left.\frac{dy_{BC}}{dx}\right|_{x=0} = s_3, \quad \theta_R = -\left.\frac{dy_1}{dx}\right|_{x=c} \tag{26}$$

In Eq. (25), the third and fourth terms in the right-hand side of the equation correspond to the change in the distance CD due to the curvatures of the upper and lower beams, respectively. For convenience, explicit expressions of the integrals appearing in Eq. (25) are given in Appendix B. Equation (24) is a nonlinear equation for Z and has to be solved numerically. Once solution Z is obtained, all the unknown constants are completely determined. The deflection δ at the point of load application is obtained from

$$\delta = y_{AB}|_{x=a_L} + y_{BC}|_{x=c_L} \tag{27}$$

2.2 Numerical Solution of Z . In this section we assume a model laminate consisting of a stainless steel beam with thickness $h_1=0.5$ mm, width $b_1=20$ mm, and Young's modulus $E_1=195.2$ GPa for the upper layer, and an aluminum beam with thickness $h_2=2$ mm, width $b_2=30$ mm, and Young's modulus $E_2=72.4$ GPa for the lower layer, and obtain numerical solutions for the critical buckling load, axial forces Z, and deflection curve. (The values of the Young's moduli are from our experiments.) The lengths of the beam and the crack are chosen to be $L=400$ mm and $c=240$ mm, respectively, and the locations of the load point and the right-hand crack tip are taken to be $d=150$ mm and $a_R=50$ mm, respectively.

Now in order to obtain the insight of the behavior of solution Z of $F(Z)=0$, we plot $F(Z)$ against Z. Figures 3(*a*)–3(*c*) show the plots of $F(Z)$ for the case when the magnitude of the applied load P is 1.0 N, 2.3 N, and 3.5 N, respectively. It is seen that when the magnitude of the load is small, there is only one solution of $F(Z)=0$, and as the load is increased the number of solutions increases. There appear three solutions for $P=3.5$ N (cf. Fig. 3(*c*)). Figures 4(*a*)–4(*c*) show the deflection curves corresponding to the solutions $Z(1)$, $Z(2)$, and $Z(3)$ of Fig. 3(*c*). It is seen that for deflection curves corresponding to solutions $Z(1)$ and $Z(3)$, the upper beam comes to the lower position of the lower beam (Fig. 4(*a*)), or a part of the upper beam overlaps the lower beam (Fig. 4(*c*)); hence, solutions $Z(1)$ and $Z(3)$ are irrelevant.

On the other hand, as shown in the deflection curves in Fig. 4(*b*), curves corresponding to $Z(2)$ does not contain any inconsistency, so that $Z(2)$ is the only relevant solution corresponding to the local buckling. Similar results were found for other values of P and therefore, the critical buckling load P_{cr} can be defined as the load at which the second solution comes to appear first. Thus, in the present case, $P_{cr}=2.3$ N as seen in Fig. 3(*b*). The relation between the load and deflection at the point of load application (P-δ curve) after the load is increased beyond the critical point may be obtained by first finding solution $Z(2)$ of Eq. (24) for several values of P and then substituting this into Eq. (27).

When the load is less than the critical buckling load, a beam will deflect, keeping mutual contact of the delaminated surfaces. In this case previous analyses [6] are effective. The deflection δ is proportional to the applied force P, and the compliance of the beam $\Phi=\delta/P$ has been given by

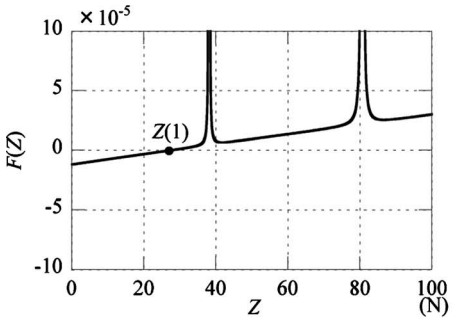

(a) P=1.0 N

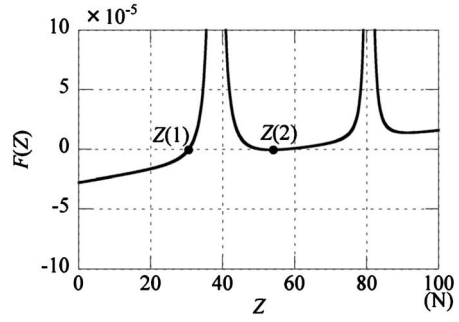

(b) P=2.3 N

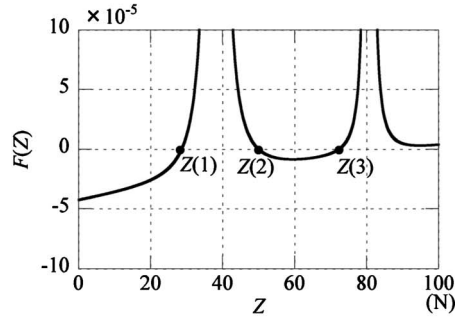

(c) P=3.5 N

Fig. 3 Plots of $F(Z)$ for several values of the applied force: (*a*) P=1.0 N, (*b*) P=2.3 N, and (*c*) P=3.5 N

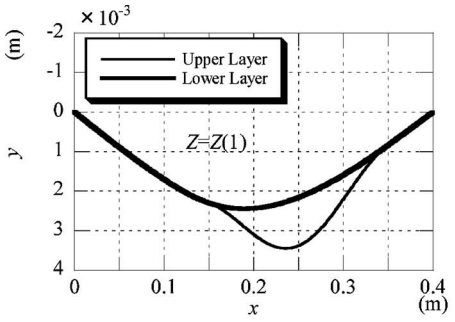

(a) $Z(1)$

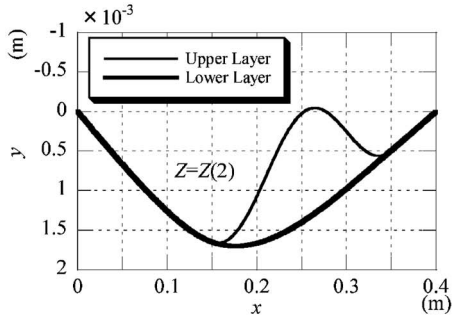

(b) $Z(2)$

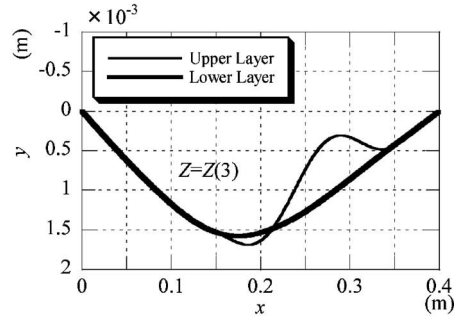

(c) $Z(3)$

Fig. 4 Deflection curves corresponding to the solution $Z(1)$, $Z(2)$, and $Z(3)$ of $F(Z)=0$ for P=3.5 N: (*a*) $Z(1)$, (*b*) $Z(2)$, and (*c*) $Z(3)$. Delamination lies between 0.11 m $\leq x \leq$ 0.35 m and loading point is at x=0.15 m.

$$\Phi = -\frac{1}{3L^2}\left(\frac{1}{D}-\frac{1}{D'}\right)[d^2(d'-c_R)^3 + d'^2(d-c_L)^3] - \frac{1}{4c}\left(\frac{1}{D}-\frac{1}{D'}\right)f^2 + \frac{d^2d'^2}{3LD} \tag{28}$$

where

$$f = [d'(2a_L + c_L)c_L + d(c_R + 2a_R)c_R]/L \tag{29}$$

Figure 5(*a*) shows the plot of the P-δ relation of the model beam, which indicates that it is nearly bilinear, and the beam becomes more flexible than it is before the delamination buckling. Figure 5(*a*) also compares the theory with the experimental results, which will be described in Sec. 4. Detailed discussions of Fig. 5 will be given in Sec. 5.

2.3 Case Where the Point of Load Application Lies Outside of the Delaminated Region. Next we consider the case where the point of load application C lies between A (the left-hand edge, or support of the beam) and B (left-hand tip of the delamination), i.e., $d < a_L$ (cf. Fig. 1). The analysis for this case becomes much easier since there is no contact region. The deflection curves for the delaminated parts of beams y_1 and y_2 with the origin of x-coordinate at the left-hand crack tip B are given as

$$y_1 = \bar{A}_1 \cos(k_1 x) + \bar{B}_1 \sin(k_1 x) - (\bar{M}_1 - F_D \bar{\alpha} x)/Z \tag{30}$$

$$y_2 = \bar{A}_2 \cosh(k_2 x) + \bar{B}_2 \sinh(k_2 x) + [\bar{M}_2 - F_D(1-\bar{\alpha})x]/Z \tag{31}$$

where expressions of $\bar{A}_i$, $\bar{B}_i$ $(i=1,2)$, $\bar{\alpha}$, and $\bar{M}_1 (=\bar{M}-\bar{M}_2)$ are given in Appendix C. The deflections for the intervals of beams AC, CB, and DF expressed as functions of x with the origin at point A are given as follows:

$$y_{AC} = -F_B x^3/(6D') + j_1 x \tag{32}$$

$$y_{CB} = \frac{F_D}{6D'}x^3 - \frac{dP}{2D'}x^2 + j_2 x + j_3 \tag{33}$$

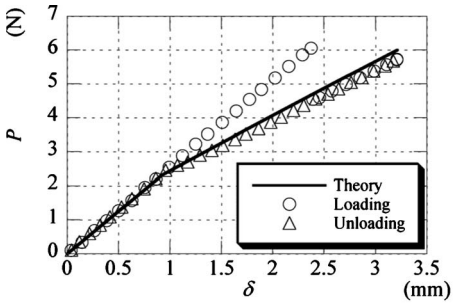

(a) $c = 240$ mm ($d \geq a_L$)

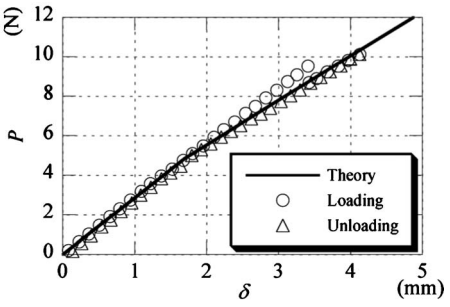

(b) $c = 160$ mm ($d \leq a_L$)

Fig. 5 Relation between the applied load *P* and the deflection at the point of load application δ: (*a*) $c=240$ mm ($d \geq a_L$); (*b*) $c=160$ mm ($d \leq a_L$)

$$y_{DF} = \frac{F_D}{6D'}x^3 - \frac{dP}{2D'}x^2 + j_4(x-L) + \frac{dPL^2}{3D'} \tag{34}$$

The constants $j_1 - j_4$ are given in Appendix C. The nonlinear equation for determining the axial force Z is given by Eqs. (24) and (25) with y_1 and y_2 replaced with Eqs. (30) and (31), and by replacing the lower limit of the integrals with 0. The explicit expressions of the results of integration are also given in Appendix C. We found that the behavior of the solutions is quite similar to the foregoing case, and the second smallest solution $Z(2)$ is the only appropriate solution for the buckling. After obtaining the solution $Z(2)$, the deflection at the load point is determined from Eq. (32) as $\delta = y_{AC}|_{x=d}$.

On the other hand when the load is less than P_{cr}, the crack faces retain mutual contact and δ is proportional to P. As have been shown in Ref. [6], when the point of load application is outside of the delaminated part, the compliance of the beam is given as

$$\Phi = \frac{d^2c^3}{12L^2}\left(\frac{1}{D} - \frac{1}{D'}\right) + \frac{d^2d'^2}{3D'L} \tag{35}$$

We take the same model beam as considered in the previous calculations. Assuming now that $c=160$ mm (with all other dimensions being kept unchanged), we calculated the load versus the deflection curve, the result of which is shown in Fig. 5(*b*). We again observe that the P-δ relation is nearly bilinear. Reflecting the fact that the length of the crack is now relatively short, the buckling load becomes large ($P_{cr}=5.0$ N) as compared with the value of 2.3 N for $c=240$ mm. Also the decrease in the slope for the post-buckling condition is not so pronounced as in Fig. 5(*a*).

For the same beam model we calculated the critical buckling load for various crack lengths. The results are shown in Fig. 6. We observe that as expected, P_{cr} decreases as the crack length is increased.

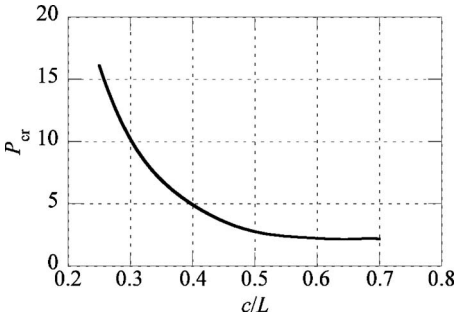

Fig. 6 Critical buckling load P_{cr} plotted for the crack length *c*/*L*

3 Energy Release Rate

One of the most important parameters characterizing the onset of the growth of delamination is the energy release rate. In this section, assuming that the widths of the upper and lower layers are equal ($b_1=b_2\equiv b$), we calculate the energy release rates for both before and after buckling states to elucidate the effect of buckling on the energy release rate. As is well known, for a specimen with the linear relation between the load and the deflection at the point of load application, the energy release rate G is given by $G=(P^2/2b)d\Phi/dc$ for crack extension under a constant load condition. Thus, when the point of load application lies on the delaminated region and delamination grows, maintaining mutual contact of cracked surfaces, then the energy release rates at the left- and right-hand tips G_{a_L} and G_{a_R}, respectively, are obtained from Eq. (28) as follows [6]:

$$G_{a_L} = \frac{P^2}{2b}\frac{d\Phi}{dc_L} = \frac{P^2c^2}{8b}\left(\frac{1}{D} - \frac{1}{D'}\right)\left[\frac{d'}{L} - \left(\frac{c_R}{c}\right)^2\right]^2 \tag{36}$$

$$G_{a_R} = \frac{P^2c^2}{8b}\left(\frac{1}{D} - \frac{1}{D'}\right)\left[\frac{d}{L} - \left(\frac{c_L}{c}\right)^2\right]^2 \tag{37}$$

In the case when the load point lies outside of the delaminated part, we have from Eq. (35) for both crack tips [6]

$$G_{a_L} = G_{a_R} = \frac{P^2d^2c^2}{8bL^2}\left(\frac{1}{D} - \frac{1}{D'}\right) \tag{38}$$

For the calculation of the energy release rate for the post-buckling condition, we utilize the formulas of Suo and Hutchinson [13]. They considered the energy release rates of a split beam with a unit width subjected to the general loading condition, as shown in Fig. 7. Applying their formulas to the present post-buckling problem, the energy release rate for the plane stress condition is given as

$$G = \frac{1}{2E_1}\left[\frac{{P_0}^2}{Ah_1} + \frac{{M_0}^2}{F{h_1}^3} + \frac{2P_0M_0}{\sqrt{AF}{h_1}^2}\sqrt{\frac{(D'-D)D_1}{(D'-D_1)D}}\right] \tag{39}$$

where

$$M_0 = ({M_1}^* - D_1M_3/D')/b \tag{40}$$

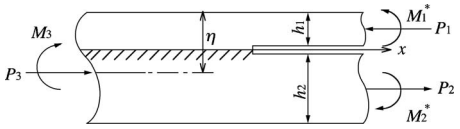

Fig. 7 Split-beam element with unit width under general loading condition (η is the distance of the neutral axis of the bonded beam from the top surface)

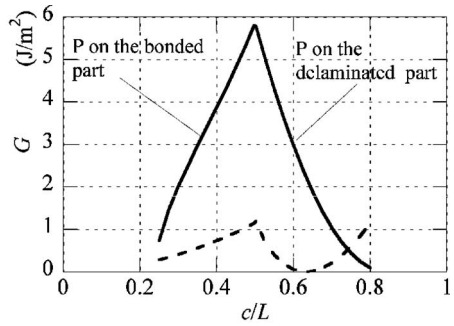

(a) left-hand tip

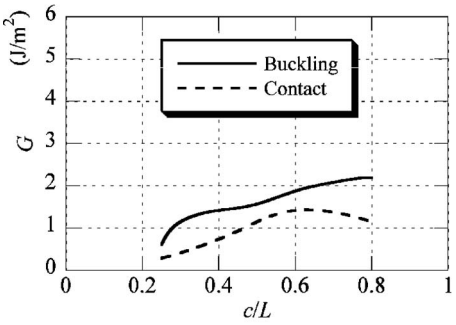

(b) right-hand tip

Fig. 8 Energy release rates: (*a*) left-hand tip; (*b*) right-hand tip

$$P_0 = [Z - hD_0M_3/(2D')]/b \tag{41}$$

with M_1^* and M_3 representing the moments pertinent to the left- and right-hand crack tips. The dimensionless constants A and F are defined by

$$A = \frac{D_0D_2}{bE_1h_1(D' - D_1)}, \quad F = \frac{D_2}{12D} \tag{42}$$

In the case where the point of application of load is on the delaminated zone, we have

$$M_1^* = D_1(F_Ba_L - hZ/2)/D, \quad M_3 = F_Ba_L \tag{43}$$

for the left-hand tip of the delamination. Likewise, the moment M_1^* for the right-hand crack tip is obtained from Eq. (12) by replacing x with c. M_3 is given by $M_3 = F_Da_R$. Quantities M_1^* and M_3 for the case where the load point lies outside of the delaminated zone may be similarly obtained.

As an example, we take the same material combination as taken in the foregoing calculations, but we now assume that the widths of the two beams are equal ($b_1 = b_2 = 30$ mm) and the height of the upper beam is assumed to be 0.4 mm. As before, the length of the beam is 400 mm, and the positions of the load application and the right-hand crack tip are fixed to be $d = 150$ mm and $a_R = 50$ mm, respectively, while the crack length is varied from 100 mm to 320 mm. The magnitude of the load is assumed to be $P = 11.0$ N, which corresponds to the critical buckling load for $c = 100$ mm.

Figure 8 shows the variation in the energy release rates at the left-hand crack tip (Fig. 8(*a*)) and right-hand crack tip (Fig. 8(*b*)) with the normalized crack length c/L. It is seen that generally the energy release rate increases by the delamination buckling, and that this effect is particularly pronounced for the left-side tip. We also note in Fig. 8(*a*) that for both buckled and contact conditions, the energy release rates increase as the crack length increases from $c = 100$ mm, and take the maximum values at $c/L = 0.5$, i.e., when the left-hand tip of the delamination coincides with the point of load application. For further increase in the crack length, the energy release rates decrease. This feature may be attributed to the closure of the crack faces near the tip due to the compression caused by the applied force.

According to Griffith's theory of fracture, the onset of delamination growth is stated as $G = G_c$, with G_c being the fracture toughness of the interface. Referring to Fig. 8, we see that if the fracture toughness of the interface G_c is relatively large, then, for example, for a crack with a length of 100 mm, the left-hand tip will extend by the buckling toward the point of load application, while the right-hand tip remains stationary, since the energy release rate at the left-hand tip is larger than that at the right-hand tip. On the other hand, if the initial crack length c/L is larger than 0.65, then the right-hand crack tip will extend, while the left-hand tip remains stationary, because in this case, the energy release rate is greater at the right-hand tip.

Generally, delamination growth is expected to occur after delamination buckling for relatively tough interface so that the assessment of delamination growth should be done based on the assumption of local buckling.

4 Experiments

We made the same steel-aluminum composite beam specimens as assumed in the analyses in Sec. 2 and conducted experiments. Thin PTFE adhesive tape with a thickness of 0.08 mm was glued on the surface of the steel beam along the prospective crack edges so that the crack edges might be made straight and normal to the axis of the beam. Two thin steel wires with a diameter of 0.04 mm (Nilaco Co., Japan) have also been spread parallel to the axes of the aluminum beams at an interval of 8 mm over the whole length of the beam prior to bonding. This manipulation was done so that the thin steel layer above the delamination would not have initial curvature, which would be induced by the gravity force. The two beams were then bonded by an epoxy binding agent Araldite (Vantico Co., Japan) except for the prospective delamination surfaces. Four composite beams containing an interface crack with lengths $c = 160$ mm, 200 mm, 240 mm, and 280 mm (all with $a_R = 50$ mm) have been prepared. A three-point flexure test ($d = 150$ mm) subject to displacement control condition was conducted using a universal testing machine (Shimazu Co., Japan). The displacement at the load point was measured by a laser displacement meter (Hioki Co., Japan).

Experimental results for the relation between P and δ for the cases of $c = 160$ mm and 240 mm have been shown in Fig. 5. As seen from these graphs, the critical buckling loads were nearly two times larger than the predicted value for the loading processes. This tendency was common to other test pieces. After the occurrence of buckling, the load immediately dropped, and after that, the P-δ relation well traced the calculated paths, as seen in Fig. 5. We also observe from Fig. 5 that for unloading processes, the load-deflection relations agree well with the calculations.

In all tests, the P-δ relations were nearly bilinear. Figure 9 summarizes the experimental results for the slopes for the cases of contact and post-buckling conditions. In the figure, Φ indicates the compliance for the condition of contact of the whole crack surfaces, whereas it indicates the inverse of the slope of the P-δ relation for the post-buckling condition. We observe that the experimental results agree well with the theoretical analyses.

5 Discussions

The characteristic feature found in the experiments is that the magnitudes of the buckling loads are generally two times larger than those predicted from the theory. For further loading after the occurrence of buckling, and in the unloading processes, experimental P-δ relations agree well with the theoretical predictions. In the present analyses, we only considered the first mode of buckling, where the contact region is fixed in the interval BC (cf. Fig. 1) and buckling occurs in the interval CD (cf. Fig. 1) with no

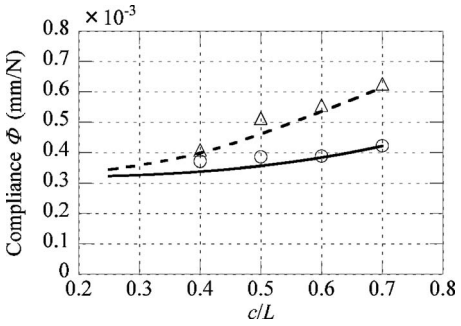

Fig. 9 Comparison of the compliances Φ between the theory and experiments. Dashed and solid line curves represent the theoretical values for post- and pre-bucklings, respectively. Triangles and circles represent the experimental results for post- and pre-bucklings, respectively.

contact occurring in this interval. Though this model is valid for the first mode of buckling, it may exclude the second mode of buckling. It is possible that the experimental buckling loads in fact indicate the load level corresponding to the second mode and that, since the second mode is unstable, the mode of deflection immediately changed to that of the first mode. The sudden drop of the applied load (from $P=6$ N to 4.5 N in Fig. 5(a) and from $P=9.5$ N to 8.5 N in Fig. 5(b)) indicates this mode change. It is inferred that, as suggested from Fig. 4(c), the second mode contains the contact region, which extends in the interval CD in Fig. 2. Hence, in a more general analysis of buckling, which covers the second mode of buckling, the contact in the buckled region CD should be taken into account, i.e., the length of the contact should be considered as an active part of the solution. The solution procedure of this generalized model would be reduced to the determination of two unknown parameters Z and the length of the contact region. The analyses of this generalized model will become somewhat involved but are necessary to fully explain the experimental results.

6 Conclusions

In this paper, on the basis of a simple beam theory, analyses were given for local delamination buckling in two-layered beams subjected to three-point bending. A nonlinear equation determining the axial forces induced by bending in the parts of the beam above and below the delaminations was derived. This equation possesses only one solution for small loads, whereas it yields more than two solutions as the applied load becomes large. By examining the deflection curves of the beam corresponding to each solution, it was concluded that the occurrence of buckling corresponds to the advent of the second solution. Thus, the critical buckling loads were defined as the load at which the second solution comes to appear first. On the other hand, for loads smaller than the critical load, our previous theory [6] assuming the contact of whole delamination surfaces is effective. Nearly bilinear relations between the applied load and deflection at the point of load application were obtained for some model laminates, which were shown to agree well with experiments.

The differences between the critical buckling loads observed in the experiments and those predicted from the theory was also discussed. A more generalized model in which the contact zones are considered as an active part of the solution was suggested, but the complete solution of this model is left for future study.

The effect of delamination buckling on the energy release rate was also studied. It was shown that due to buckling the energy release rate generally takes values much greater than those for the case of perfect contact of the crack faces. The energy release rate will become even greater if buckling occurs in the second mode. It is expected that generally, for relatively tough interfaces, delamination will extend through delamination buckling. Hence, the assessment of the strength of the interface of the composite beams should be made by taking delamination buckling into consideration.

Acknowledgment

This work was supported by the Ministry of Education, Science, Sports, and Culture of Japan (Grant in Aid for Scientific Research (C), Grant No. 17560073).

Appendix A

From the conditions of continuity of deflections and the slopes at points B, C, and D, we have

$$\left.\frac{dy_{AB}}{dx}\right|_{x=a_L} = \left.\frac{dy_{BC}}{dx}\right|_{x=0} \quad \text{at B} \tag{A1}$$

$$y_{BC}|_{x=d-a_L} = y_1|_{x=d-a_L} = y_2|_{x=d-a_L} \quad \text{at C} \tag{A2}$$

$$\left.\frac{dy_{BC}}{dx}\right|_{x=d-a_L} = \left.\frac{dy_1}{dx}\right|_{x=d-a_L} = \left.\frac{dy_2}{dx}\right|_{x=d-a_L} \quad \text{at C} \tag{A3}$$

$$y_1|_{x=c} = y_2|_{x=c}, \quad y_{AB}|_{x=a_L} + y_1|_{x=c} = y_{DF}|_{x=a_L+c} \quad \text{at D} \tag{A4}$$

$$\left.\frac{dy_1}{dx}\right|_{x=c} = \left.\frac{dy_2}{dx}\right|_{x=c} = \left.\frac{dy_{DF}}{dx}\right|_{x=a_L+c} \quad \text{at D} \tag{A5}$$

We note that Eqs. $(A2_2)$, $(A3_2)$, $(A4_1)$, and $(A5_1)$ contain only A_i and B_i $(i=1,2)$. Thus we solve Eqs. $(A2_2)$ and $(A3_2)$ for A_1 and B_1 to express them as functions of A_2 and B_2. Then substituting into Eqs. $(A4_1)$ and $(A5_1)$ and solving, we have A_2 and B_2. In this way we have

$$A_1 = a_1 \sin\theta + (a_2 - a_3)\cos\theta, \quad B_1 = a_1 \cos\theta - (a_2 - a_3)\sin\theta \tag{A6}$$

$$A_2 = (\delta_1 a_{22} - \delta_2 a_{12})/\Delta, \quad B_2 = (-\delta_1 a_{21} + \delta_2 a_{11})/\Delta \tag{A7}$$

where

$$\theta = k_1(d - a_L), \quad a_1 = A_2\Gamma + B_2/\Gamma + [M + F_B(d - a_L)]/Z \tag{A8}$$

$$a_2 = (k_2/k_1)(A_2\Gamma - B_2/\Gamma), \quad a_3 = (P - F_B)/k_1 Z \tag{A9}$$

$$a_{11} = [\cos(k_1\bar{e}) + (k_2/k_1)\sin(k_1\bar{e})]\Gamma - \exp(k_2 c) \tag{A10}$$

$$a_{12} = [\cos(k_1\bar{e}) - (k_2/k_1)\sin(k_1\bar{e})]/\Gamma - \exp(-k_2 c) \tag{A11}$$

$$a_{21} = [\sin(k_1\bar{e}) - (k_2/k_1)\cos(k_1\bar{e})]\Gamma + (k_2/k_1)\exp(k_2 c) \tag{A12}$$

$$a_{22} = [\sin(k_1\bar{e}) + (k_2/k_1)\cos(k_1\bar{e})]/\Gamma - (k_2/k_1)\exp(-k_2 c) \tag{A13}$$

$$\delta_1 = [M + cF_B - \bar{e}P + \{(P - F_B)\sin(k_1\bar{e})\}/k_1 - \{M + F_B(d - a_L)\}\cos(k_1\bar{e})]/Z \tag{A14}$$

$$\delta_2 = -\frac{M + F_B(d - a_L)}{Z}\sin(k_1\bar{e}) + \frac{(P - F_B)}{k_1 Z}(1 - \cos(k_1\bar{e})) \tag{A15}$$

$$\Delta = a_{11}a_{22} - a_{12}a_{21} \tag{A16}$$

with

$$\Gamma = \exp[k_2(d - a_L)], \quad \bar{e} = a_L + c - d$$

$$M = M_1 + M_2 = F_B a_L - Zh/2 \tag{A17}$$

The remaining unknowns may be readily obtained from the rest of the equations. Thus, $s_3 - s_5$, α_1', and α_2 are given as functions of Z as follows:

$$s_3 = J_1 - \alpha_1' F_B/Z, \quad s_4 = s_3 + F_B a_L^2/(2D') \tag{A18}$$

$$s_5 = k_1(A_1 \cos(k_1 c) - B_1 \sin(k_1 c)) + f_2 + \frac{-\alpha_1' F_B + \alpha_2 P}{Z} - \frac{Pd(a_L + c)^2}{2LD'} + \frac{Pd(a_L + c)}{D'} \tag{A19}$$

$$\alpha_2 = \frac{Z}{P}[J_1 + 3s_1(d - a_L)^2 + 2s_2(d - a_L) - f_2 - k_1(A_1 \cos\theta - B_1 \sin\theta)]$$

$$\beta_2 = 1 - \alpha_2 \tag{A20}$$

$$\alpha_1' = -ZJ_2/(F_B L), \quad \beta_1' = 1 - \alpha_1' \tag{A21}$$

where

$$J_1 = [A_1 \sin\theta + B_1 \cos\theta - M_1/Z - f_1]/(d - a_L) + f_2 - s_1(d - a_L)^2 - s_2(d - a_L) \tag{A22}$$

$$J_2 = \frac{Pd(a_L + c)^3}{6LD'} - \frac{Pd(a_L + c)^2}{2D'} + [k_1(A_1 \cos(k_1 c) - B_1 \sin(k_1 c)) + f_2 + \alpha_2 P/Z - Pd(a_L + c)^2/(2LD') + Pd(a_L + c)/D'] \times (a_L + c - L) + \frac{PdL^2}{3D'} + \frac{F_B a_L^3}{6D'} - \left(J_1 + \frac{F_B a_L^2}{2D'}\right) a_L - A_1 \sin(k_1 c) - B_1 \cos(k_1 c) + (M_1 - \alpha_2 P\bar{e})/Z + f_1 - f_2 c \tag{A23}$$

Appendix B

The results of the integrals in Eq. (25) and the angles of inclination at the tip of the delamination (Eq. (26_2)) are given as follows:

$$\int_{d-a_L}^{c} (y_1')^2 dx = [k_1^2(A_1^2 + B_1^2)/2 + H_1^2 + f_2^2 + 2f_2 H_1]\bar{e} + k_1[A_1 B_1\{\cos(2k_1 c) - \cos(2\theta)\}/2 + (A_1^2 - B_1^2) \times \{\sin(2k_1 c) - \sin(2\theta)\}/4] + 2(H_1 + f_2) \times [A_1 \sin(k_1 c) + B_1 \cos(k_1 c) - A_1 \sin\theta - B_1 \cos\theta] \tag{B1}$$

$$\int_{d-a_L}^{c} (y_2')^2 dx = \{H_2^2 + f_2^2 - 2f_2 H_2 - 2A_2 B_2 k_2^2\}\bar{e} + (k_2/2) \times [A_2^2 \exp(2k_2 c) - B_2^2 \exp(-2k_2 c) - A_2^2 \exp\{2k_2(d - a_L)\} + B_2^2 \exp\{-2k_2(d - a_L)\}] - 2(H_2 - f_2)[A_2 \exp(k_2 c) + B_2 \exp(-k_2 c) - A_2 \exp\{k_2(d - a_L)\} - B_2 \exp\{-k_2(d - a_L)\}] \tag{B2}$$

where

$$H_1 = (-\alpha_1' F_B + \alpha_2 P)/Z, \quad H_2 = (-\beta_1' F_B + \beta_2 P)/Z \tag{B3}$$

The explicit expression of the angle of inclination θ_R is

$$\theta_R = -y_1'|_{x=c} = -k_1\{A_1 \cos(k_1 c) - B_1 \sin(k_1 c)\} + \alpha_1' F_B/Z - f_2 - \alpha_2 P/Z \tag{B4}$$

Appendix C

The constants appearing in Eqs. (30) and (31) are given as follows:

$$\bar{A}_1 = \bar{M}_1/Z, \quad \bar{A}_2 = -\bar{M}_2/Z \tag{C1}$$

$$\bar{B}_1 = \frac{F_D(F_4 F_5 - F_2 F_3) + \bar{M}(F_3 F_5 - F_2 F_6)}{Z(F_1 F_5 + k_1 F_2^2)} \tag{C2}$$

$$\bar{B}_2 = (\bar{B}_1 k_1 + F_D/Z)/k_2 \tag{C3}$$

$$\bar{M}_1 = \frac{F_D(k_1 F_2 F_4 + F_1 F_3) + \bar{M}(k_1 F_2 F_3 + F_1 F_6)}{F_1 F_5 + k_1 F_2^2}, \quad \bar{M}_2 = \bar{M} - \bar{M}_1 \tag{C4}$$

where

$$F_1 = \sin(k_1 c) - (k_1/k_2)\sinh(k_2 c), \quad F_2 = \cos(k_1 c) - \cosh(k_2 c) \tag{C5}$$

$$F_3 = 1 - \cosh(k_2 c), \quad F_4 = (1/k_2)\sinh(k_2 c) - c \tag{C6}$$

$$F_5 = k_1 \sin(k_1 c) + k_2 \sinh(k_2 c), \quad F_6 = k_2 \sinh(k_2 c) \tag{C7}$$

$$\bar{M} = F_D(L - a_L) - Zh/2 \tag{C8}$$

The constants appearing in Eqs. (32)–(34) are given as follows:

$$j_1 = j_2 - d^2 P/(2D'), \quad j_2 = k_1 \bar{B}_1 + F_D\left(\frac{\bar{\alpha}}{Z} - \frac{a_L^2}{2D'} + \frac{a_L L}{D'}\right) \tag{C9}$$

$$j_3 = -Pd^3/(6D') \tag{C10}$$

$$j_4 = -(\bar{M}_1 k_1/Z)\sin(k_1 c) + \bar{B}_1 k_1 \cos(k_1 c) + \frac{F_D \bar{\alpha}}{Z} - \frac{F_D}{2D'}(a_L + c)^2 + \frac{dP}{D'}(a_L + c) \tag{C11}$$

where

$$\bar{\alpha} = \frac{Z}{dP}\left[\frac{F_D}{6D'}\{(a_L + c)^3 + 2a_L^3 + 3a_R(a_L + c)^2\} + \frac{dP}{6D'}\{2L^2 + d^2 - 3a_L^2 - 3(a_L + c)^2 - 6a_R(a_L + c)\} - \bar{B}_1\{\sin(k_1 c) + k_1 a_L + k_1 a_R \cos(k_1 c)\} + \frac{\bar{M}_1}{Z}\{1 - \cos(k_1 c) + k_1 a_R \sin(k_1 c)\}\right] \tag{C12}$$

The integrals appearing in the nonlinear equation are given as follows:

$$\int_0^c (y_1')^2 dx = \frac{(\bar{M}_1 k_1)^2}{2Z^2}\left(c - \frac{\sin(2k_1 c)}{2k_1}\right) + \frac{(\bar{B}_1 k_1)^2}{2}\left(\frac{\sin(2k_1 c)}{2k_1} + c\right) + \left(\frac{\bar{\alpha} F_D}{Z}\right)^2 c + \frac{2\bar{B}_1 \bar{\alpha} F_D}{Z}\sin(k_1 c) + \frac{\bar{M}_1 k_1 \bar{B}_1}{2Z}(\cos(2k_1 c) - 1) + \frac{2\bar{M}_1 \bar{\alpha} F_D}{Z^2}(\cos(k_1 c) - 1) \tag{C13}$$

$$\int_0^c (y_2')^2 dx^2 = \frac{(\bar{M}_2 k_2)^2}{2Z^2}\left(\frac{\sin(2k_2c)}{2k_2} - c\right) + \frac{(\bar{B}_2 k_2)^2}{2}\left(\frac{\sinh(2k_2c)}{2k_2} + c\right) + (1-\bar{\alpha})^2 c\left(\frac{F_D}{Z}\right)^2 - \frac{2\bar{B}_2(1-\bar{\alpha})F_D}{Z}\sinh(k_2c) + \frac{\bar{M}_2 k_2 \bar{B}_2}{2Z}(1-\cosh(2k_2c)) + \frac{2(1-\bar{\alpha})\bar{M}_2 F_D}{Z^2}(\cosh(k_2c)-1) \quad \text{(C14)}$$

References

[1] Maikuma, H., Gillespie, J. W., Jr., and Whitney, J. M., 1989, "Analysis and Experimental Characterization of the Center Notch Flexural Test Specimen for Mode II Interlaminar Fracture," J. Compos. Mater., **23**(8), pp. 756–786.

[2] Suemasu, H., and Majima, O., 1996, "Multiple Delaminations and Their Severity in Circular Axisymmetric Plates Subjected to Transverse Loading," J. Compos. Mater., **30**(4), pp. 441–453.

[3] Suemasu, H., and Majima, O., 1998, "Multiple Delaminations and Their Severity in Nonlinear Circular Plates Subjected to Concentrated Loading," J. Compos. Mater., **32**(2), pp. 123–140.

[4] Hutchinson, J. W., and Lu, T. J., 1995, "Laminate Delamination due to Thermal Gradients," ASME J. Eng. Mater. Technol., **117**(4), pp. 386–390.

[5] Toya, M., Oda, M., Kado, A., and Saitoh, T., 2005, "Energy Release Rates for an Edge Delamination of a Laminated Beam Subjected to Thermal Gradient," ASME J. Appl. Mech., **72**(5), pp. 658–665.

[6] Toya, M., Aritomi, M., and Chosa, A., 1997, "Energy Release Rates for an Interface Crack Embedded in a Laminated Beam Subjected to Three-Point Bending," ASME J. Appl. Mech., **64**(2), pp. 375–382.

[7] Chai, H., Babcock, C. D., and Knauss, W. G., 1981, "One Dimensional Modeling of Failure in Laminated Plates by Delamination Buckling," Int. J. Solids Struct., **17**(11), pp. 1069–1083.

[8] Bottega, W. J., and Maewal, A., 1983, "Delamination Buckling and Growth in Laminates," ASME J. Appl. Mech., **50**(1), pp. 184–189.

[9] Yin, W.-L., 1985, "Axisymmetric Buckling and Growth of a Circular Delamination in a Compressed Laminate," Int. J. Solids Struct., **21**(5), pp. 503–514.

[10] Madenci, E., and Westman, R. A., 1991, "Local Delamination Buckling in Layered Systems," ASME J. Appl. Mech., **58**(1), pp. 157–166.

[11] Madenci, E., and Westman, R. A., 1993, "Local Delamination Growth in Layered Systems Under Compressive Load," ASME J. Appl. Mech., **60**(4), pp. 895–902.

[12] Kardomateas, G. A., 1993, "The Initial Post-Buckling and Growth Behavior of Internal Delaminations in Composite Plates," ASME J. Appl. Mech., **60**(4), pp. 903–910.

[13] Suo, Z., and Hutchinson, J. W., 1990, "Interface Crack Between Two Elastic Layers," Int. J. Fract., **43**(1), pp. 1–18.